

---

This is an electronic reprint of the original article.

This reprint may differ from the original in pagination and typographic detail.

Hyypä, E.; Jenei, M.; Masuda, S.; Sevriuk, V.; Tan, K. Y.; Silveri, M.; Goetz, J.; Partanen, M.; Lake, R. E.; Grönberg, L.; Möttönen, M.

## Calibration of cryogenic amplification chains using normal-metal-insulator-superconductor junctions

*Published in:*  
Applied Physics Letters

*DOI:*  
[10.1063/1.5096262](https://doi.org/10.1063/1.5096262)

Published: 13/05/2019

*Document Version*  
Publisher's PDF, also known as Version of record


*Please cite the original version:*

Hyypä, E., Jenei, M., Masuda, S., Sevriuk, V., Tan, K. Y., Silveri, M., Goetz, J., Partanen, M., Lake, R. E., Grönberg, L., & Möttönen, M. (2019). Calibration of cryogenic amplification chains using normal-metal-insulator-superconductor junctions. *Applied Physics Letters*, 114(19), 1-5. Article 192603.  
<https://doi.org/10.1063/1.5096262>

# Calibration of cryogenic amplification chains using normal-metal–insulator–superconductor junctions

Cite as: Appl. Phys. Lett. **114**, 192603 (2019); <https://doi.org/10.1063/1.5096262>

Submitted: 15 March 2019 . Accepted: 30 April 2019 . Published Online: 17 May 2019

E. Hyypä , M. Jenei , S. Masuda , V. Sevriuk , K. Y. Tan , M. Silveri , J. Goetz , M. Partanen , R. E. Lake , L. Grönberg, and M. Möttönen 



View Online



Export Citation



CrossMark

## ARTICLES YOU MAY BE INTERESTED IN

[Fast control of dissipation in a superconducting resonator](#)

Applied Physics Letters **115**, 082601 (2019); <https://doi.org/10.1063/1.5116659>

[A quantum engineer's guide to superconducting qubits](#)

Applied Physics Reviews **6**, 021318 (2019); <https://doi.org/10.1063/1.5089550>

[Frequency-tunable high-Q superconducting resonators via wireless control of nonlinear kinetic inductance](#)

Applied Physics Letters **114**, 192601 (2019); <https://doi.org/10.1063/1.5098466>

Lock-in Amplifiers  
Find out more today



 Zurich Instruments

AIP  
Publishing

# Calibration of cryogenic amplification chains using normal-metal-insulator-superconductor junctions

Cite as: Appl. Phys. Lett. **114**, 192603 (2019); doi: [10.1063/1.5096262](https://doi.org/10.1063/1.5096262)

Submitted: 15 March 2019 · Accepted: 30 April 2019 ·

Published Online: 17 May 2019



View Online



Export Citation



CrossMark

E. Hyypä,<sup>1,a)</sup> M. Jenei,<sup>1,a),b)</sup> S. Masuda,<sup>1,2</sup> V. Sevriuk,<sup>1</sup> K. Y. Tan,<sup>1,3</sup> M. Silveri,<sup>1,4</sup> J. Goetz,<sup>1</sup> M. Partanen,<sup>1</sup> R. E. Lake,<sup>1</sup> L. Grönberg,<sup>5</sup> and M. Möttönen<sup>1</sup>

## AFFILIATIONS

<sup>1</sup>QCD Labs, QTF Centre of Excellence, Department of Applied Physics, Aalto University, P.O. Box 13500, FI-00076 Aalto, Finland

<sup>2</sup>College of Liberal Arts and Sciences, Tokyo Medical and Dental University, Ichikawa 272-0827, Japan

<sup>3</sup>Center for Quantum Computation and Communication Technology, School of Electrical Engineering and Telecommunications, University of New South Wales, Sydney, NSW 2052, Australia

<sup>4</sup>Research Unit of Nano and Molecular Systems, University of Oulu, P.O. Box 3000, FI-90014 Oulu, Finland

<sup>5</sup>VTT Technical Research Centre of Finland, QFT Center of Excellence, P.O. Box 1000, FI-02044 Aalto, Finland

<sup>a)</sup>Contributions: E. Hyypä and M. Jenei contributed equally to this work.

<sup>b)</sup>Electronic mail: [mate.jenei@aalto.fi](mailto:mate.jenei@aalto.fi)

## ABSTRACT

Various applications of quantum devices call for an accurate calibration of cryogenic amplification chains. To this end, we present an experimentally feasible calibration scheme and use it to accurately measure the total gain and noise temperature of an amplification chain by employing normal-metal-insulator-superconductor (NIS) junctions. Our method is based on the radiation emitted by inelastic electron tunneling across voltage-biased NIS junctions. We derive an analytical expression that relates the generated power to the applied bias voltage which is the only control parameter of the device. After the setup has been characterized using a standard voltage reflection measurement, the total gain and the noise temperature are extracted by fitting the analytical expression to the microwave power measured at the output of the amplification chain. The  $1\sigma$  uncertainty of the total gain of 51.84 dB appears to be of the order of 0.10 dB.

© 2019 Author(s). All article content, except where otherwise noted, is licensed under a Creative Commons Attribution (CC BY) license (<http://creativecommons.org/licenses/by/4.0/>). <https://doi.org/10.1063/1.5096262>

Superconducting circuits provide a promising approach to implement a variety of quantum devices and to explore fundamental physical phenomena, such as the light-matter interaction<sup>1</sup> in the ultrastrong coupling regime.<sup>2–4</sup> In addition, superconducting circuits are potential candidates for building a large-scale quantum computer:<sup>5,6</sup> superconducting qubits can be coupled in a scalable way,<sup>7–14</sup> and both the gate and the measurement fidelity of qubits exceed the threshold required for quantum error correction.<sup>12,15–17</sup>

Since superconducting quantum circuits typically operate in the single-photon regime, signals are amplified substantially for read-out<sup>5,18–23</sup> using a chain of amplifiers, which is distributed over several temperature stages.<sup>18,19</sup> In the first stage, a near-quantum-limited amplifier,<sup>24</sup> such as a Josephson parametric amplifier,<sup>25–28</sup> is often used to lower the noise temperature of the amplification chain.<sup>29</sup> As a result of cascading several amplifiers, the uncertainty in the total gain of the amplification chain becomes significant and may complicate, for example, the estimation of the photon number in the superconducting

circuit. Therefore, accurate, fast, and simple methods for measuring the total gain of an amplification chain are desirable in the investigation of quantum electric devices.

The gain and the noise temperature of cryogenic amplifiers can be measured, for example, using superconducting qubits,<sup>24,30</sup> Planck spectroscopy of a subkelvin thermal noise source,<sup>31</sup> and the Y-factor method<sup>32,33</sup> which utilizes the Johnson-Nyquist noise emitted at different temperatures. In addition to these methods, shot noise<sup>34,35</sup> sources, such as normal-metal-insulator-normal-metal junctions, can be used to determine the gain and noise temperature of cryogenic amplifiers.<sup>36,37</sup> However, this method typically requires a calibration measurement of the setup due to impedance mismatch.<sup>36</sup>

In this paper, we present an accurate alternative calibration scheme for the total gain and noise temperature of an amplification chain by utilizing photon-assisted electron tunneling in normal-metal-insulator-superconductor (NIS) junctions. To date, NIS junctions have been utilized in various applications, which include, for

example, cryogenic microwave sources,<sup>38</sup> thermometers,<sup>39,40</sup> and the recently developed quantum-circuit refrigerator that cools quantum electric circuits by harnessing photon-assisted electron tunneling.<sup>41–43</sup> Here, we determine the gain and noise temperature of an amplification chain by measuring the power emitted by electrons that tunnel inelastically across NIS junctions. The photon emission of the tunneling electrons can be activated by applying a bias voltage across the NIS junctions. For our analysis, we derive an analytical expression for the generated power in the high-bias regime. The analytical model matches our experimental results, which allows us to determine the gain of the amplification with an uncertainty of the order of 0.10 dB.

We demonstrate the proposed calibration scheme on a sample illustrated in Fig. 1. The device incorporates a superconductor–insulator–normal-metal–insulator–superconductor (SINIS) junction which consists of two NIS junctions sharing a common normal-metal electrode. The normal-metal electrode of the tunnel junction is capacitively coupled ( $C_c$ ) to a half-wavelength superconducting coplanar-waveguide LC resonator. The resonator is further capacitively coupled ( $C_g$ ) to a transmission line from its other end, which conducts the signal to a three-stage amplification chain. The sample is placed in a dry dilution refrigerator at a 10-mK base temperature. Reference 38 details the device fabrication. Since our focus is to introduce a calibration scheme in general, benchmarking the amplifiers separately is out of the scope of this paper.

The bias voltage  $V_b$  across the SINIS junction activates the photon-assisted electron tunneling events which control the mean photon number  $N_r$  in the fundamental mode of the weakly coupled

resonator.<sup>41</sup> The photon number in turn determines the microwave power emitted to the transmission line. As described in Fig. 2, the electrons can tunnel through the NIS junction either elastically, i.e., without energy exchange with their electromagnetic environment, or inelastically by emitting or absorbing photons. In our setup, the resonator acts as the electromagnetic environment, and consequently, the tunneling electrons absorb or emit photons at the resonance frequency of the resonator  $f_r = \omega_r/(2\pi) = 4.67$  GHz.

For vanishing bias voltage, both the elastic and inelastic tunneling events are suppressed due to the energy gap<sup>44–46</sup> of  $2\Delta$  in the superconductor density of states as shown in Fig. 2(a). If the bias voltage is slightly below the energy gap, i.e.,  $|eV_b| \lesssim 2\Delta$ , electrons can tunnel through the junction by absorbing photons from the environment, which results in cooling of the resonator mode. In this work, we are mostly interested in the high-bias-voltage regime  $|eV_b| \gg 2\Delta$ , where electron tunneling events involving photon emission are greatly enhanced, and hence, the resonator mode heats up. The elevated temperature of the resonator mode leads to an increased radiative power into the transmission line, which enables us to calibrate the total gain of the amplification chain.

We show below that the power and the bias voltage relate to each other through a simple equation in the high-bias regime. We apply the theory developed in Ref. 42 to describe the coupling between the resonator and the SINIS junction. In this model, we only take into account single-photon processes and assume that the quasiparticle temperatures are equal in the normal-metal and superconducting electrodes. Furthermore, we assume sequential tunneling, i.e., that high-order processes are suppressed by the opaque tunnel barrier. Using the simplified electric circuit in Fig. 1(b) and Fermi's golden rule, we can express the resonator damping rate  $\gamma_T$  and the effective temperature  $T_T$  owing to the electron tunneling across the SINIS junction as<sup>42</sup>

$$\gamma_T = \bar{\gamma}_T \frac{\pi}{\omega_r} \sum_{l, \tau = \pm 1} l \bar{F}(\tau eV + l\hbar\omega_r), \quad (1)$$

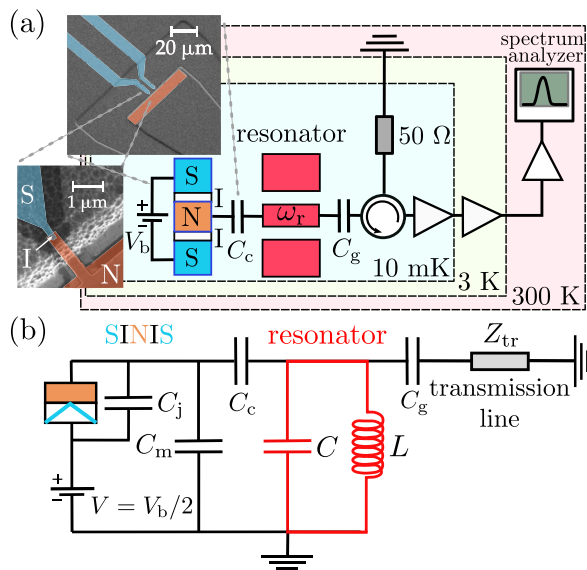


**FIG. 1.** (a) Schematic of the measurement setup. A bias voltage  $V_b$  is applied across an SINIS junction, which is coupled to a resonator through capacitance  $C_c$ . The other end of the resonator is coupled through capacitance  $C_g$  to a transmission line, whose characteristic impedance is  $Z_{tr} = 50 \Omega$ . The insets show false-color scanning electron micrographs of a NIS junction. (b) A simplified electric circuit diagram of the system depicted in panel (a). The capacitor  $C_j$  describes the capacitance of a single NIS junction, whereas the capacitor  $C_m$  corresponds to the remaining capacitance. The fundamental mode of the resonator is modeled as an LC oscillator.

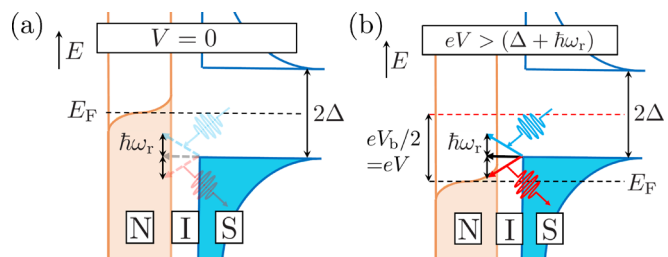


**FIG. 2.** (a) Sketch of the occupied (shaded) and unoccupied (white) quasiparticle states in an NIS junction at vanishing bias voltage. In the normal metal (orange), the occupation is given by the Fermi–Dirac distribution since the density of states is essentially constant in the energy scale of interest. In the superconducting electrode (blue), there is an energy gap of  $2\Delta$  in the density of states, which restricts the possible electron tunneling events. Straight blue arrows indicate tunneling events involving photon (wavy arrow) absorption, whereas red arrows correspond to photon emission, and black arrows depict elastic tunneling events. The low transparency of the arrows highlights that all the above-mentioned tunneling events are suppressed. (b) As (a) but for a bias voltage  $eV > \Delta + \hbar\omega_r$  causing the Fermi level  $E_F$  of the normal metal (black dashed line) to shift with respect to that of the superconductor (red dashed line).

$$T_T = \frac{\hbar\omega_r}{k_B} \left\{ \ln \left[ \frac{\sum_{\tau=\pm 1} \tilde{F}(\tau eV + \hbar\omega_r)}{\sum_{\tau=\pm 1} \tilde{F}(\tau eV - \hbar\omega_r)} \right] \right\}^{-1}, \quad (2)$$

where  $\bar{\gamma}_T$  is the asymptotic damping rate,  $\tilde{F}(E)$  is the normalized rate of forward tunneling,  $k_B$  is the Boltzmann constant,  $\hbar$  is the reduced Planck constant, and  $V = V_b/2$  is the voltage across a single NIS junction. We also have  $\bar{\gamma}_T = 2C_c^2 Z_r \omega_r / [(C_c + C_j + C_m)^2 R_T]$ , where  $Z_r = \sqrt{L/C}$ ,  $R_T$  is the tunneling resistance of a single NIS junction, and the remaining symbols are defined in Fig. 1(b). The normalized rate of forward tunneling is defined as

$$\tilde{F}(E) = \frac{1}{2\pi\hbar} \int d\varepsilon n_S(\varepsilon) \frac{f(\varepsilon - E) - f(\varepsilon)}{1 - e^{-E/(k_B T_N)}}, \quad (3)$$

where  $E$  is the energy gained by the tunneling electron,  $T_N$  is the temperature of the normal-metal electrode,  $f(\varepsilon) = \{\exp[\varepsilon/(k_B T_N)] + 1\}^{-1}$  is the Fermi function, and  $n_S(\varepsilon)$  is the Dynes density of states,<sup>45</sup> which can be written as  $n_S(\varepsilon) = |\text{Re}[(\varepsilon + i\gamma_D \Delta) / \sqrt{(\varepsilon + i\gamma_D \Delta)^2 - \Delta^2}]|$ . The Dynes parameter  $\gamma_D$  describes the broadening of the superconductor energy gap and is of the order of  $\sim 10^{-4}$  in a typical experimental scenario.<sup>38,41,47</sup>

In the high-bias regime,  $eV \gg \Delta$ , we employ Eqs. (1) and (2) to derive the following approximations for the damping rate  $\gamma_T$  and the effective photon number  $N_T = \{\exp[\hbar\omega_r/(k_B T_T)] - 1\}^{-1}$  of the engineered environment:

$$\gamma_T \approx \bar{\gamma}_T \left[ 1 + \frac{1}{2} \frac{\Delta^2}{(eV)^2} \right], \quad (4)$$

$$N_T \approx \frac{eV}{2\hbar\omega_r} - \frac{1}{2} - \frac{\Delta^2}{2\hbar\omega_r eV}, \quad (5)$$

where we have utilized the Sommerfeld expansion. In addition, we have assumed that the Dynes parameter is small enough to be neglected at high-bias voltages.

The resonator exchanges energy with the SINIS junction and with the transmission line. Furthermore, the resonator may be subjected to additional sources of dissipation which we model as a single excess reservoir. Each of these three types of dissipation can be modeled as a virtual transmission line,<sup>48</sup> which allows us to write the net power flow between the resonator and the  $i$ th dissipative reservoir as

$$P_i = \hbar\omega_r \gamma_i (N_i - N_r), \quad (6)$$

where  $\gamma_i$  is the damping rate of the resonator owing to the  $i$ th reservoir,  $N_i$  is the corresponding effective photon number, and  $N_r$  is the resulting steady-state occupation of the resonator. Invoking the power balance and using Eqs. (4) and (5), the net power flow into the transmission line can be approximated as

$$P_{tr} \approx \frac{\gamma_{tr} \bar{\gamma}_T}{\gamma_{tr} + \bar{\gamma}_T + \gamma_x} \left\{ \frac{eV}{2} + \hbar\omega_r \left[ \frac{\gamma_x (N_x - N_r)}{\bar{\gamma}_T} - N_r - \frac{1}{2} \right] - \frac{1}{4} \frac{\Delta^2}{eV} \left( 1 + \frac{\bar{\gamma}_T}{\gamma_{tr} + \gamma_x} \right) \right\}, \quad (7)$$

where  $\gamma_{tr}$  and  $N_{tr}$  are the damping rate and the effective photon number owing to the transmission line, respectively, whereas  $\gamma_x$  and  $N_x$  are the corresponding quantities for the excess losses.

In our experiments, we measure the output power of the amplification chain  $P_{out} = GP_{tr} + P_{noise}$ , where  $G$  is the total gain of the amplification chain including possible attenuation and losses, and  $P_{noise}$  is the noise power originating from the amplifiers. Consequently, we can determine the total gain  $G$  by fitting a function of the form

$$P_{out}(V) = aV + b + c/V \quad (8)$$

to the measured power in the high-bias regime  $eV \gg \Delta$ , where  $\{a, b, c\}$  are the fitting parameters. Using Eq. (7), the total gain  $G$  can be expressed in terms of the leading-term coefficient as

$$G = \frac{2a \bar{\gamma}_T + \gamma_{tr} + \gamma_x}{e \bar{\gamma}_T \gamma_{tr}}. \quad (9)$$

Although we extract the total gain only from the coefficient  $a$ , the other terms in Eq. (8) improve the fit substantially. The effective noise temperature of the system  $T_s$ , which includes the noise caused by the incident power from the transmission line, the spectrum analyzer, and the amplification chain, is obtained by examining the output power at zero-bias voltage  $P_{out}(0)$ , where  $P_{tr}$  is practically zero with our device parameters and consequently

$$T_s = \frac{P_{out}(0)}{Gk_B \Delta f}, \quad (10)$$

where  $\Delta f$  is the bandwidth of the amplification chain.

In our experiments, we characterize the damping rates  $\bar{\gamma}_T$ ,  $\gamma_{tr}$ , and  $\gamma_x$  with high accuracy leaving the parameter  $a$  in Eq. (9) as the only free parameter in our model. To this end, we conduct standard microwave reflection measurements at different bias voltages  $V_b$ , which involves all possible impedance mismatches in the system. Based on the input-output theory,<sup>49</sup> the voltage reflection coefficient of our system can be written as<sup>50</sup>

$$\Gamma = \frac{(2-r)\gamma_{tr} - r(\gamma_T + \gamma_x) + 2ir(\omega_p - \omega_r)}{\gamma_T + \gamma_{tr} + \gamma_x - 2i(\omega_p - \omega_r)}, \quad (11)$$

where  $\omega_p/(2\pi)$  is the probe frequency and  $r$  is a complex-valued Fano resonance correction factor, which arises from the direct cross-talk of the dissipative reservoirs.<sup>51</sup>

Since the bias voltage  $V_b$  controls the coupling between the electromagnetic environment, which is formed by the photon-assisted electron tunneling across the NIS junction, and the resonator, a Lamb shift arises for the resonance frequency  $f_r$ .<sup>43</sup> The Lamb shift provides a convenient way of eliminating the unwanted background from the measurement data, namely, normalizing by the zero-bias measurement trace  $\Gamma^N(V_b) = \Gamma(V_b)/\Gamma(0)$  as shown in Fig. 3(a). The ratio of two instances of Eq. (11) is fitted for every  $V_b$  above the critical coupling point,  $eV_b/(2\Delta) > 1$ , where the bias voltage-independent  $\gamma_{tr}$ ,  $\gamma_x$ , and the bias voltage-dependent  $\gamma_T$  are fitting parameters. Next, the asymptotic damping rate is extracted using Eq. (4). As a result, our characteristic damping rates are  $\gamma_{tr}/(2\pi) = (1.78 \pm 0.02)$  MHz,  $\bar{\gamma}_T/(2\pi) = (17.39 \pm 0.04)$  MHz, and  $\gamma_x/(2\pi) = (0.46 \pm 0.01)$  MHz, where the presented  $1\sigma$  uncertainties are obtained by the following method: First, an error circle is created that has a radius equal to the root mean square fit error and the center is located at  $\Gamma^N(V_b, \omega_r)$ , which correspond to the resonance of the bias voltage-dependent feature. Then, the confidence intervals of each parameter are individually determined by finding the boundaries such that the fitted  $\Gamma^N$  is located within the



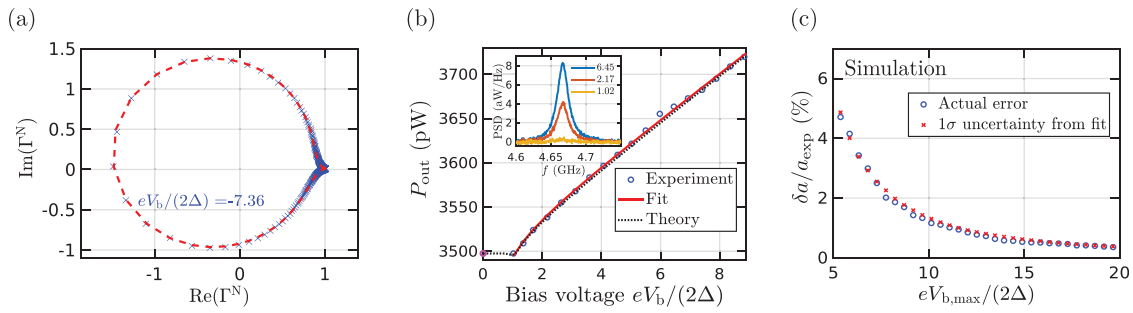


**FIG. 3.** (a) Example of the normalized complex voltage reflection coefficient  $\Gamma^N$  (blue crosses) and a fit (red dashed line) according to Eq. (11). (b) The measured output power  $P_{\text{out}}$  as a function of the bias voltage (blue dots), a fit to Eq. (8) (red line), and the theoretically predicted power (dotted black line). The magenta circle illustrates the system noise at zero-bias. The inset shows the differences in the power spectral densities (PSDs) at zero and finite bias voltages. Each PSD is averaged over 100 frequency sweeps. (c) The average relative error of the fitting parameter  $a$  (blue dots) and the average  $1\sigma$  uncertainty given by the fit (red crosses) as a function of the upper bound of the fitting range  $eV_b/(2\Delta) \in [1.07, eV_{b,\text{max}}/(2\Delta)]$ .

error circle. The uncertainty of the excess damping rate is taken as the standard deviation of  $\gamma_x$  over the fitted voltage range.

After measuring the damping rates, we determine the total gain of the amplification chain by recording the microwave power at the output of the amplification chain for different bias voltages across the junction. To this end, we use a spectrum analyzer and numerically integrate the averaged power spectral density around the resonance frequency in the range of 4.6–4.75 GHz. From the data shown in Fig. 3(b), we observe a monotonous increase in the microwave power if the bias voltage exceeds the energy gap. We finally extract the total gain of the amplification chain by fitting Eq. (8) to the power data in the voltage range  $eV_b/(2\Delta) \in [1.07, 8.83]$ . Using Eq. (9) and the experimentally determined device parameters, the total gain of the amplification chain is estimated to be  $G = 51.84$  dB. Combining the fitted total gain and the theoretical prediction for the generated microwave power that is calculated using Eqs. (1), (2), and (6), we find a good agreement between experiment and theory. The power at  $|eV_b|/(2\Delta) < 1.07$  yields 11 K for the system noise temperature based on Eq. (10) in the range of 4.6–4.75 GHz. We have estimated the zero-bias transmission line temperature according to Ref. 38 and found its contribution negligible to  $T_s$ , as is the case for the spectrum analyzer. Thus, we attribute the unexpectedly high value for the system noise temperature to an atypical operation of a HEMT amplifier in the chain. Fortunately, this phenomenon does not hinder our ability to demonstrate the introduced calibration method.

The relative uncertainty of the fitting parameter  $a$  is extracted in the following way: we substitute the damping rates and the calibrated gain into Eq. (9) to determine the expected value  $a_{\text{exp}}$  for the fitting parameter  $a$ . Then, we create 100 simulated power datasets for bias voltages up to  $V_b = 10 \Delta/e$ . The simulated power data are obtained by adding normally distributed random noise to the exact theoretical prediction for the power calculated using Eqs. (1), (2), and (6). The standard deviation of the random noise  $\sigma = 2.5$  pW and the spacing between consecutive voltage points are chosen to coincide with the data shown in Fig. 3(b). By fitting Eq. (8) to the corresponding power values, we extract the parameter  $a$  and record the absolute error  $\delta a = a - a_{\text{exp}}$  as a function of the maximum bias  $eV_{b,\text{max}}/(2\Delta)$ . In addition, we obtain the  $1\sigma$  uncertainty from the fit and observe that it agrees with the error  $\delta a$  shown in Fig. 3(c). In our experiments, we reach  $eV_b/2\Delta = 9$  and therefore estimate the relative uncertainty of

the fitting parameter  $\delta a/a_{\text{exp}} = 2\%$ . By combining the uncertainties of the damping rates  $\bar{\gamma}_T$ ,  $\gamma_{tr}$ ,  $\gamma_x$ , and the fitting parameter  $a$ , we acquire 0.10 dB for the uncertainty of the total gain.

In this paper, we have presented a calibration scheme for the total gain and noise temperature of a general amplification chain that comprises cryogenic and noncryogenic amplifiers. Currently, our setup allows the calibration of the total gain only at frequencies corresponding to a mode frequency of the resonator. The frequency range suitable for calibration can be expanded by placing a superconducting quantum interference device (SQUID) in the resonator.<sup>52,53</sup> In the future, we aim at benchmarking the accuracy of the proposed gain calibration scheme against a method utilizing a superconducting qubit in a resonator. By employing the ac Stark shift, we can determine the photon number in the resonator<sup>1,54</sup> and thus the total gain of the amplification chain.

This project received funding from the European Union's Horizon 2020 Research and Innovation Programme under the Marie Skłodowska-Curie Grant Agreement No. 795159 and under the European Research Council Consolidator Grant No. 681311 (QUESS), from the Academy of Finland Centre of Excellence in Quantum Technology Grant Nos. 312300 and 305237, from JST ERATO Grant No. JPMJER1601, from JSPS KAKENHI Grant No. 18K03486, and from the Vilho, Yrjö and Kalle Väisälä Foundation. We acknowledge the provision of facilities and technical support by Aalto University at OtaNano - Micronova Nanofabrication Centre.

## REFERENCES

1. A. Wallraff, D. I. Schuster, A. Blais, L. Frunzio, R.-S. Huang, J. Majer, S. Kumar, S. M. Girvin, and R. J. Schoelkopf, *Nature* **431**, 162 (2004).
2. T. Niemczyk, F. Deppe, H. Huebl, E. Menzel, F. Hocke, M. Schwarz, J. Garcia-Ripoll, D. Zueco, T. Hümmer, E. Solano *et al.*, *Nat. Phys.* **6**, 772 (2010).
3. X. Gu, A. F. Kockum, A. Miranowicz, Y. X. Liu, and F. Nori, *Phys. Rep.* **718**, 1 (2017).
4. A. F. Kockum, A. Miranowicz, S. De Liberato, S. Savasta, and F. Nori, *Nat. Rev. Phys.* **1**, 19 (2019).
5. M. H. Devoret and R. J. Schoelkopf, *Science* **339**, 1169 (2013).
6. A. Blais, R.-S. Huang, A. Wallraff, S. M. Girvin, and R. J. Schoelkopf, *Phys. Rev. A* **69**, 062320 (2004).
7. J. Majer, J. Chow, J. Gambetta, J. Koch, B. Johnson, J. Schreier, L. Frunzio, D. Schuster, A. Houck, A. Wallraff *et al.*, *Nature* **449**, 443 (2007).

- <sup>8</sup>M. A. Sillanpää, J. I. Park, and R. W. Simmonds, *Nature* **449**, 438 (2007).
- <sup>9</sup>L. DiCarlo, J. Chow, J. Gambetta, L. S. Bishop, B. Johnson, D. Schuster, J. Majer, A. Blais, L. Frunzio, S. Girvin *et al.*, *Nature* **460**, 240 (2009).
- <sup>10</sup>L. DiCarlo, M. D. Reed, L. Sun, B. R. Johnson, J. M. Chow, J. M. Gambetta, L. Frunzio, S. M. Girvin, M. H. Devoret, and R. J. Schoelkopf, *Nature* **467**, 574 (2010).
- <sup>11</sup>T. Brecht, W. Pfaff, C. Wang, Y. Chu, L. Frunzio, M. H. Devoret, and R. J. Schoelkopf, *npj Quantum Inf.* **2**, 16002 (2016).
- <sup>12</sup>R. Barends, J. Kelly, A. Megrant, A. Veitia, D. Sank, E. Jeffrey, T. C. White, J. Mutus, A. G. Fowler, B. Campbell *et al.*, *Nature* **508**, 500 (2014).
- <sup>13</sup>A. D. Córcoles, E. Magesan, S. J. Srinivasan, A. W. Cross, M. Steffen, J. M. Gambetta, and J. M. Chow, *Nat. Commun.* **6**, 6979 (2015).
- <sup>14</sup>C. Song, K. Xu, W. Liu, C.-P. Yang, S.-B. Zheng, H. Deng, Q. Xie, K. Huang, Q. Guo, L. Zhang *et al.*, *Phys. Rev. Lett.* **119**, 180511 (2017).
- <sup>15</sup>D. S. Wang, A. G. Fowler, and L. C. Hollenberg, *Phys. Rev. A* **83**, 020302 (2011).
- <sup>16</sup>J. Kelly, R. Barends, A. Fowler, A. Megrant, E. Jeffrey, T. White, D. Sank, J. Mutus, B. Campbell, Y. Chen *et al.*, *Nature* **519**, 66 (2015).
- <sup>17</sup>N. Ofek, A. Petrenko, R. Heeres, P. Reinhold, Z. Leghtas, B. Vlastakis, Y. Liu, L. Frunzio, S. Girvin, L. Jiang *et al.*, *Nature* **536**, 441 (2016).
- <sup>18</sup>F. Mallet, F. R. Ong, A. Palacios-Laloy, F. Nguyen, P. Bertet, D. Vion, and D. Esteve, *Nat. Phys.* **5**, 791 (2009).
- <sup>19</sup>A. Dews, F. Ong, V. Schmitt, R. Lauro, N. Boulant, P. Bertet, D. Vion, and D. Esteve, *Phys. Rev. Lett.* **108**, 057002 (2012).
- <sup>20</sup>Z. Lin, K. Inomata, W. Oliver, K. Koshino, Y. Nakamura, J. Tsai, and T. Yamamoto, *Appl. Phys. Lett.* **103**, 132602 (2013).
- <sup>21</sup>D. Riste, M. Dukalski, C. Watson, G. De Lange, M. Tiggelman, Y. M. Blanter, K. W. Lehnert, R. Schouten, and L. DiCarlo, *Nature* **502**, 350 (2013).
- <sup>22</sup>J. Heinsoo, C. K. Andersen, A. Remm, S. Krinner, T. Walter, Y. Salathé, S. Gasparinetti, J.-C. Besse, A. Potočník, A. Wallraff *et al.*, *Phys. Rev. Appl.* **10**, 034040 (2018).
- <sup>23</sup>J. Ikonen, J. Goetz, J. Ilves, A. Kernen, A. M. Gunyhó, M. Partanen, K. Y. Tan, L. Grönberg, V. Vesterinen, S. Simbierowicz *et al.*, *Phys. Rev. Lett.* **122**, 080503 (2019).
- <sup>24</sup>C. Macklin, K. O'Brien, D. Hover, M. Schwartz, V. Bolkhovskiy, X. Zhang, W. Oliver, and I. Siddiqi, *Science* **350**, 307 (2015).
- <sup>25</sup>B. Yurke, P. Kaminsky, R. Miller, E. Whittaker, A. Smith, A. Silver, and R. Simon, *Phys. Rev. Lett.* **60**, 764 (1988).
- <sup>26</sup>T. Yamamoto, K. Inomata, M. Watanabe, K. Matsuba, T. Miyazaki, W. Oliver, Y. Nakamura, and J. Tsai, *Appl. Phys. Lett.* **93**, 042510 (2008).
- <sup>27</sup>M. Castellanos-Beltran and K. Lehnert, *Appl. Phys. Lett.* **91**, 083509 (2007).
- <sup>28</sup>S. Pogorzalek, K. G. Fedorov, L. Zhong, J. Goetz, F. Wulschner, M. Fischer, P. Eder, E. Xie, K. Inomata, T. Yamamoto *et al.*, *Phys. Rev. Appl.* **8**, 024012 (2017).
- <sup>29</sup>R. Kokkonen, J. Govenius, V. Vesterinen, R. Lake, A. Gunyhó, K. Tan, S. Simbierowicz, L. Grönberg, J. Lehtinen, M. Prunnila *et al.*, preprint [arXiv:1806.09397](https://arxiv.org/abs/1806.09397) (2018).
- <sup>30</sup>J. Goetz, S. Pogorzalek, F. Deppe, K. G. Fedorov, P. Eder, M. Fischer, F. Wulschner, E. Xie, A. Marx, and R. Gross, *Phys. Rev. Lett.* **118**, 103602 (2017).
- <sup>31</sup>M. Mariani, E. P. Menzel, F. Deppe, M. A. Caballero, A. Baust, T. Niemczyk, E. Hoffmann, E. Solano, A. Marx, and R. Gross, *Phys. Rev. Lett.* **105**, 133601 (2010).
- <sup>32</sup>Noise Figure Measurement Accuracy - The Y-Factor Method - Application Note (Keysight Technologies, 2018) available at <http://literature.cdn.keysight.com/litweb/pdf/5952-3706E.pdf>.
- <sup>33</sup>J. Fernandez, "A noise-temperature measurement system using a cryogenic attenuator," in TMO Progress Report 42-135, November 5, 1998.
- <sup>34</sup>Y. M. Blanter and M. Büttiker, *Phys. Rep.* **336**, 1 (2000).
- <sup>35</sup>L. Spietz, K. Lehnert, I. Siddiqi, and R. Schoelkopf, *Science* **300**, 1929 (2003).
- <sup>36</sup>S.-W. Chang, J. Aumentado, W.-T. Wong, and J. C. Bardin, in *IEEE MTT-S International Microwave Symposium (IMS)*, 2016 (IEEE, 2016), pp. 1-4.
- <sup>37</sup>A. Aassime, G. Johansson, G. Wendin, R. Schoelkopf, and P. Delsing, *Phys. Rev. Lett.* **86**, 3376 (2001).
- <sup>38</sup>S. Masuda, K. Y. Tan, M. Partanen, R. E. Lake, J. Govenius, M. Silveri, H. Grabert, and M. Möttönen, *Sci. Rep.* **8**, 3966 (2018).
- <sup>39</sup>S. Kafanov, A. Kemppinen, Y. A. Pashkin, M. Meschke, J. Tsai, and J. P. Pekola, *Phys. Rev. Lett.* **103**, 120801 (2009).
- <sup>40</sup>S. Gasparinetti, K. Viisanen, O.-P. Saira, T. Faivre, M. Arzeo, M. Meschke, and J. Pekola, *Phys. Rev. Appl.* **3**, 014007 (2015).
- <sup>41</sup>K. Y. Tan, M. Partanen, R. E. Lake, J. Govenius, S. Masuda, and M. Möttönen, *Nat. Commun.* **8**, 15189 (2017).
- <sup>42</sup>M. Silveri, H. Grabert, S. Masuda, K. Y. Tan, and M. Möttönen, *Phys. Rev. B* **96**, 094524 (2017).
- <sup>43</sup>M. Silveri, S. Masuda, V. Sevriuk, K. Y. Tan, M. Jenei, E. Hyppä, F. Hassler, M. Partanen, J. Goetz, R. E. Lake, L. Grönberg, and M. Möttönen, "Broadband Lamb shift in an engineered quantum system," *Nat. Phys.* (published online).
- <sup>44</sup>J. Bardeen, L. N. Cooper, and J. R. Schrieffer, *Phys. Rev.* **108**, 1175 (1957).
- <sup>45</sup>R. Dynes, J. Garno, G. Hertel, and T. Orlando, *Phys. Rev. Lett.* **53**, 2437 (1984).
- <sup>46</sup>I. Giaever, *Phys. Rev. Lett.* **5**, 147 (1960).
- <sup>47</sup>J. P. Pekola, V. Maisi, S. Kafanov, N. Chekurov, A. Kemppinen, Y. A. Pashkin, O.-P. Saira, M. Möttönen, and J. Tsai, *Phys. Rev. Lett.* **105**, 026803 (2010).
- <sup>48</sup>J. Goetz, F. Deppe, P. Eder, M. Fischer, M. Müting, J. P. Martínez, S. Pogorzalek, F. Wulschner, E. Xie, K. G. Fedorov *et al.*, *Quantum Sci. Technol.* **2**, 025002 (2017).
- <sup>49</sup>C. Gardiner and M. Collett, *Phys. Rev. A* **31**, 3761 (1985).
- <sup>50</sup>A. A. Clerk, M. H. Devoret, S. M. Girvin, F. Marquardt, and R. J. Schoelkopf, *Rev. Mod. Phys.* **82**, 1155 (2010).
- <sup>51</sup>S. Fan, W. Suh, and J. D. Joannopoulos, *J. Opt. Soc. Am. A* **20**, 569 (2003).
- <sup>52</sup>M. Partanen, K. Y. Tan, S. Masuda, J. Govenius, R. E. Lake, M. Jenei, L. Grönberg, J. Hassel, S. Simbierowicz, V. Vesterinen *et al.*, *Sci. Rep.* **8**, 6325 (2018).
- <sup>53</sup>M. Sandberg, C. Wilson, F. Persson, T. Bauch, G. Johansson, V. Shumeiko, T. Duty, and P. Delsing, *Appl. Phys. Lett.* **92**, 203501 (2008).
- <sup>54</sup>D. Schuster, A. Wallraff, A. Blais, L. Frunzio, R.-S. Huang, J. Majer, S. Girvin, and R. Schoelkopf, *Phys. Rev. Lett.* **94**, 123602 (2005).